A Dual- Stator Machine with Diametrically Magnetized PM: Analytical Air-gap Flux Calculation, Efficiency Optimization and Comparison with Conventional Dual-Stator Machines

Shahin Asgari [a,*], Reza Yazdanpanah [b], Mojtaba Mirsalim[a]

[a] Electrical Machines and Transformers Research Laboratory, Electrical Engineering Department, Amirkabir University of Technology, Tehran, Iran. (email: asgari_shahin@aut.ac.ir, mirsalim@aut.ac.ir)

[b] Department of Electrical Engineering, University of Larestan, Lar, Iran (email: ryazdanpanah@lar.ac.ir)

[*]corresponding author (tel: +989183378515, Postal code: 1591634311)

Abstract: This paper presents a design and optimization procedure for a dual-stator machine with a diametrically magnetized PM to improve the electromagnetic performance. First, analytical design equations are presented based on MEC analysis; they are used to design a basic dual-stator machine. Then, by applying an artificial intelligence algorithm, the machine is optimized to achieve high efficiency and torque density, and low pulsating torque for direct-drive applications. A quantitative comparison is performed between the optimized new machine and conventional dual-stator machines to evaluate the performances and improvements of the understudy machine. The machine performance, including air-gap flux density distribution, back electromotive force, electromagnetic torque, cogging torque, and torque ripple are analyzed by the finite element method. The analysis results have demonstrated that benefiting from its topology, the optimized dual-stator machine with diametrically magnetized PM has the comprehensively better performance, including higher torque density, higher efficiency, and lower torque ripple and cogging torque compared to conventional dual-stator machines.

Keywords: analytical design, dual-stator, finite element method, optimization, PM machine, torque

1. Introduction

Permanent magnet synchronous machines (PMSMs) have been investigated for various requests such as industrial, transportation, renewable energy and direct-drive applications due to their high torque density, high power density, high power

factor and efficiency [1-3]. Because of better utilization of materials and high performance, three-phase PMSMs are the most common for the mentioned applications [1]. The dual air-gap PMSMs such as dual-stator PM synchronous machines (DS-PMSM) [4-7] and dual-rotor PM machines [8-11] offer much higher power density than the conventional ones because of the total output torque results from the torque components produced by the interactions in two air-gap flux densities.

Lately, various DS-PMSM machines are being researched [1], [12-16] that provide better performances over the previously introduced machines. Spoke-type electrical machines have been found useful because of their enhanced torque density and flux focusing effects. A dual-stator spoke-type Vernier machine (DSSTVM) realizes a flux-focusing effect on Vernier machines and so, achieves a high value of power factor. However, DSSTVM only focused on this factor for the Vernier machine. In [17-18], high-temperature superconductor bulks were utilised in the PM Vernier machine to shield the leakage flux and increase the torque density.

Also, cogging torque is one of the primary drawbacks of PMSMs, especially for low speed and direct-drive applications which results in vibration and acoustic noise [19].

A novel topology for DS-PMSM has been introduced in [4]. In this paper, first, an analytical model for air-gap flux density calculation in a variable thickness DS-PMSM is presented and verified by a numerical method. This model could be used for the primary design objectives. Then, the structure optimization is investigated to find the appropriate motor for high torque and low-speed applications.

A comparative study of the new proposed DS-PMSM [4] and previously researched machines is performed for high torque and low-speed applications, where the critical parameters are torque ripple, cogging torque, torque density and efficiency. To disclose the characteristics, the finite element method (FEM) analysis is used.

2. Machine Topology and Field Calculations

Fig. 1 shows a dual-stator permanent magnet synchronous machine with diametrically magnetized cylindrical PMs (DMCPMs) that is an alternative for a DS-PMSM with surface mounted PMs and has advantages such as [4]:

- Higher mechanical strength
- Lower torque ripple
- Sinusoidal air-gap flux density distribution
- Less construction cost

Fig. 2 shows that the inner stator flux crosses the air-gap and the PM and then, enters the outer stator before closing the path in the adjacent pole.

A smaller thickness at the edges compared to the centre of a PM results in a lower tooth-torque and the PM leakage flux [4] (fig. 3).

2.1. Air-gap Flux Density Calculation Using MEC

The variable PM thickness changes the trapezoidal flux density distribution to a sinusoidal. In most models of the magnetic equivalent circuit (MEC) for PM machines, the PM is represented by a flux source and a reluctance [20]. Because of the varying PM thickness, such models are not accurate enough to determine the air-gap flux density distribution.

So, a new approach will be proposed in this section for these structures, and the results will be compared using the FEM analysis results.

Fig. 4 shows one pole pair of the machine, where, R_s , R_l , ϕ_r and R_m are the stator reluctance, leakage flux path reluctance, flux source and the PM reluctance, respectively. The simplified MEC is in fig. 5a, where the PM flux, air-gap flux and leakage flux are shown by ϕ , ϕ_g and ϕ_l , respectively.

It is not easy to determine an analytical equation for the leakage reluctance, but the air gap flux can be written in terms of the magnetic flux as $\varphi_g = K_l \varphi$ where, K_l is a leakage factor that is typically a little less than one. In other words, the leakage reluctance can be eliminated by using this relationship. For the motor with surface PMs, the leakage factor is typically in the range of $0.9 < K_l \leq 1$. Because of the saturation characteristic of ferromagnetic materials, the steel reluctance (R_s) is nonlinear. Therefore, this reluctance must be eliminated in some way to find an analytical solution. As the permeability of the steel is high, the steel reluctance is small in comparison to the air gap reluctance R_g .That is, the steel reluctance can be eliminated by introducing a reluctance factor K_r . Here K_r is a constant that increases the air gap reluctance slightly to consider steel reluctance. The reluctance factor is in the range of $1.0 < K_r \leq 1.2$ [20].

It is important to note that determining an accurate analytical expression for the leakage and reluctance factors complicates the proposed model. These values are usually chosen based on the experience. Therefore, in this study, the mean value of their ranges are selected to simplifying the proposed model ($K_l = 0.95, K_r = 1.1$). Final simplified MEC results, as shown in fig. 5b.

2.2. MEC Calculations

Using fig. 5, the flux is calculated by:

$$\phi = \frac{2R_m}{2R_m + 4k_r R_g}\phi_r = \frac{1}{1 + 2k_r R_g / R_m}\phi_r \qquad (1)$$

Considering:

$$R_m = \frac{l_m}{\mu_r \mu_0 A_m},\ R_g = \frac{g}{\mu_0 A_g} \qquad (2)$$

results in:

$$\phi_g = k_l \phi = \frac{k_l}{1 + 2k_r \frac{\mu_r g A_m}{l_m A_g}} \phi_r \qquad (3)$$

where, A_m, l_m, g, A_g are the PM cross-section area and thickness, and the air-gap length and cross-section area, respectively.

Using:

$$B_g = \frac{\phi_g}{A_g},\ B_r = \frac{\phi_r}{A_m},\ c = \frac{A_m}{A_g},\ p = \frac{l_m}{g.c} \qquad (4)$$

the air-gap flux density is:

$$B_g(x) = \frac{k_l c}{1 + 2k_r \frac{\mu_r}{p}} B_r \qquad (5)$$

The PM to air-gap area coefficient, or flux concentration factor c is equal to 1 for surface mounted PM machines [20]. For the current topology with a stack length of L, and considering fig. 6, it is calculated as follows:

$$A_m = r\pi L, A_g = w_t L \ \rightarrow \ c = \frac{r\pi}{w_t} \qquad (6)$$

In addition, the effect of open slots of the stator is handled by the Carter coefficient. In other words, the real air gap is replaced by an equivalent air gap [21].

For the variable thickness PM machine shown in fig. 6, the corresponding air-gap length and PM thickness are related to each other as in Equation 7. This equation is used in Equation 5 to calculate the air-gap flux density at each point.

$$l_m(x) = \sqrt{r^2 - x^2}, g(x) = r + d - l_m(x)\ ; \qquad -r \le x \le r \qquad (7)$$

2.3. Flux Density Distribution Verification and Machine Dimensions

Using Equation 5, for a basic machine, the air-gap flux density distribution results as shown in fig. 7. This figure also compares the analytical results with the numerical field calculations by FEM that verifies the accuracy of the proposed

analytical method. Also, the peak flux density calculated by the MEC is exactly coincident with the numerical analysis. The discrepancy in the two ends of the magnetic flux density distribution is due to the flux fringing effect, as the proposed model simplifies the magnetic circuit to reduce the calculations.

If the machine is designed to have no saturation in critical points, linear behavior in the whole range of operation would be achieved. So, the average magnetic flux density in the mentioned points that are inner and outer stators are calculated as:

$$B_{sat.s} = \frac{\phi_g}{l_s L} \qquad (8)$$

Here, l_s and L are the stators yoke thickness and the machine axial length, respectively. In the design process, $B_{sat.s}$ should be kept below the saturation point.

3. Machine Design and Optimization

3.1. Design Algorithm

In this subsection, the design algorithm is explained step by step. Fig. 8 depicts the flowchart of the design process with the main values tabulated in Table 1.

3.1.1. Design Criteria

There are some specific constraints for design of electric machines in every application. The maximum current density, the maximum flux densities in the teeth and the yoke, and the maximum temperature are some of the most important limitations. In the first step, the required design specifications for the proposed machine should be determined. Here, the design variables are chosen as the radii of the inner and outer air-gap, the number of slots, and the pole-arc to pole-pitch ratio. The final values are given in Table 1.

3.1.2. Number of poles and the pole-arc width

The length of pole-arc is the main difficulty in using DMCPMs for designing DS-PMSMs, especially in the low-number of pole-pair structures. As fig. 2 shows, increasing the pole-arc results in higher thickness of PMs. To overcome this, one approach is to increase the number of poles, which decreases the mechanical pole-arc angle. Here, according to the maximum speed of the application and the width of the pole-arc, the number of poles is selected.

3.1.3. Slot width, combinations of the numbers of slots and poles, and winding layout

By using the results of section two, it can be concluded that the most reduction of the cogging torque appears where the diameter of the PM is equal or smaller than the width of the tooth [4]. The appropriate diameter of the PM can be realized by using the fractional slot structure with the number of slots per-pole per-phase less than unity ($q < 1$).

Equation (9) shows the cogging torque goodness factor,

$$C = \frac{2PN_s}{N_c} \tag{9}$$

where, if C is small, the cogging torque will be low [22]. Here, P is the number of pole pairs, N_s the number of slots, and N_C the smallest common multiplier of numbers of slots and numbers of poles. In general, there are two types of winding configuration: distributed and concentrated. The concentrated winding is more appropriate for this structure due to its advantages following reasons [23]:

- fractional slot structure
- slots per-pole per-phase less than unity ($q < 1$)
- high power and efficiency
- short end winding and consequently, less copper loss
- increased torque to current ratio due to the high slot fill factor

It should be noted that the concentrated winding produces harmonics in the air-gap magneto-motive force (mmf) that increases iron loss in the rotor, especially in non-laminated structures. Here, due to the use of aluminum in the structure of the proposed rotor, the iron losses of the rotor are neglected.

3.1.4. The air-gap radii and flux density

The design algorithm has a loop for the number of poles, the air-gap radius, the air-gap flux density, and the PM thickness and to calculate the inner and outer air-gap radii. Air-gap flux density is calculated by 2nd section equations. It should be mentioned that this algorithm is not suitable for the low-pole structures with the number of poles smaller than 12.

3.1.5. Back-EMF and torque characteristics

After satisfying the air-gap flux density, the primary machine characteristics, such as the cogging torque, torque ripple, the average torque, and the efficiency are calculated. If the results are acceptable, the process will be finished. If not, the process will go back to the first step, and the design constraints will be changed within the allowable range until the design goals are satisfied.

3.2. Optimization Approach

For high torque and low-speed applications, the essential characteristics are air-gap flux density, back EMF, torque density, efficiency, and losses. Dual-stator machines inherently have a higher torque density compared to single-stator machines as the produced torque is the sum of the two air-gap torques.

The principal objective of the DMCPM optimization is machine efficiency, but the cogging torque and torque ripple and density are considered as the constraints in this process.

The primary design parameter that affects the machine performance is the rotor radius. This parameter determines the rotor position between the two stators. For a constant PM radius, the rotor radius defines the PM arc to pole arc ratio (α) that affects the torque ripple and cogging torque directly [24].

In the understudy machine, the magnetic circuits of inner and outer stators are in series. Also, the electrical circuits of the stators are in series with the same currents in the windings. The rotor radius determines the slot area and hence the magnetic flux of the two stators. The flux has a significant effect on the machine produced torque and copper loss.

Other optimization parameters are inner and outer stator tooth width that determines the winding space, and subsequently the loss and efficiency. The optimization goal is to maximize efficiency with the constraints that are presented in Table 2.

For the mentioned objectives and constraints, the designed DMCPM machine has been optimized using the well-known procedure GA [25].

The initial and optimal values of the geometrical parameters are presented in Table 3.

3.3. Optimization Results

Fig. 9 shows the flux density distribution, where the tooth maximum flux density is about 1.1T. The back electromotive force and the cogging torque are presented in figs. 10 and 11 that show an increase of 11.7% in the back EMF and the cogging torque from 0.27% to 0.7% in the optimized machine. The higher cogging torque is due to the rotor radius increase, but still is considerably low.

Fig. 12 compares the electromagnetic torque of the machines, where it shows a 2.2% increase in the average torque and a 42% decrease in the torque ripple.

It is remarkable that although the cogging torque has increased, the total torque ripple has improved in the optimized machine.

Table 4 summarizes the initial and optimal design parameters. Besides, the comparison of the performance parameters, including efficiency, torque density, back EMF, and losses are presented.

4. Comparison with Other Topologies

There are recently proposed DS-PMSM machines that have special advantages over previous versions. In this section, machines with similar power ratings are presented and discussed.

4.3. Dual-stator spoke-type interior PM machine (S-IPMM) with spoke-type configurations using phase-group concentrated coil (PGCC) windings

A dual-stator S-IPMM is having 24 stator slots (S), and 26 magnet poles (P) with PGCC windings has been proposed in [14]. The two stators in the proposed machine are misaligned by one tooth width. Ferrite PMs are used which are arranged as a spoke-type array with the alternately reversing magnetization direction. Steel sheets of NSSMC 50H470 are utilized for the ferromagnetic parts of the machine.

When the rotor pole rotates to become aligned with the teeth of the stator, nearly all the PM flux corresponding to one phase group will flow into one air-gap for improved air-gap flux density. After the $\pi/2$ electrical rotation, the same effects will occur in the other air-gap where the PM flux flows into two air gaps simultaneously. So, a highly improved air-gap flux density results in a higher subsequent torque compared to the conventional dual air-gap machines in which the two air gaps work independently.

4.4. A novel dual-stator Vernier permanent magnet machine

The proposed machine has two stators and a sandwiched rotor [15]. The outer stator is a conventional stator with three-phase windings and semi-closed slots, and the inner stator has an iron core, and surface mounted PMs on it. The rotor has a consequent-pole structure with Halbach-array PMs.

The proposed machine can be observed as a superposition of two machines: single-stator PM machine (Machine I: the consequent-pole PM rotor and the outer stator) and a double-stator VPM machine (Machine II: the inner stator, the reluctance rotor, and the outer stator). Because of the self-shielding effect of the Halbach-array magnets, the rotor back iron is not needed for Machine I.

4.5. Dual-stator consequent-pole permanent magnet Vernier machine

In the configuration of the proposed machine [12], there are two stators and a sandwiched rotor. But, some key differences are that in the inner stator, as an alternative of surface-mounted PMs, consequent-pole PMs are used, which reduces

the PM volume. The machine can also be considered as a combination of two machines. The structure, including an outer stator, sandwiched rotor, and inner stator iron teeth are termed machine I, whereas the structure comprising an outer stator, iron teeth in the rotor, and the complete inner stator is named machine II. In the proposed machine, machines I and II are both dual-stator Vernier machines, which increases the torque density.

The key novelty of the proposed topology is its working principle, where the flux of both rotor and inner stator PMs is modulated, and the back EMF is induced in the winding of the outer stator.

4.6. An optimized dual- stator machine with diametrically magnetized PM

The machine designed and optimized in the 3rd section of this paper has been compared with other machines (A to C) in the performances. Table 5 summarizes the results, where the key parameters are torque ripple, cogging torque, torque density, and efficiency.

The torque density of machine D is 208-331% higher, which means that when the same torques are desired for all machines, the active volume of machine D can be 52-70% smaller compared to machines A to C.

Table 5 shows that machine D contains at least 65% less cogging torque than other machines based on the FEM results.

The torque ripple of machine D obtained from the torque superposition of the two air-gaps, reduced by 73-95% compared to that of the other machines.

Efficiency is also a significant performance index. It is found that the efficiency of machine D is 2-20% higher than that of machines A to C.

Totally, machine D exhibits significantly improved torque density, torque ripple and cogging torque, and acceptable improved efficiency.

5. Conclusion

This paper presented the air-gap flux density distribution analysis, design, and optimization of a dual-stator machine with the diametrically magnetized PMs has been presented. After presenting the analytical study of the machine and verification of the analytical solution, the machine was optimized for some output characteristics using artificial intelligence. Then, a quantitative comparison was carried out between the investigated machines with the aid of the 3D FEM. These comparisons showed that the optimized understudy machine had at least 208% higher torque density, 2% higher efficiency, and lower pulsating torque.

The analyses verified that the optimized dual-stator machine with the diametrically magnetized PM had significant improvements in electromagnetic performances, and so is suitable for direct-drive applications.

6. References

[1] Zhao, W., Lipo, T. A., Kwon, B. "Dual-Stator Two-Phase Permanent Magnet Machines With Phase-Group Concentrated-Coil Windings for Torque Enhancement", *IEEE Trans. Magn*., 51(11), (2015).

[2] Cupertino, F., Leuzzi, R., Monopoli, V. G., et al. "Maximisation of power density in permanent magnet machines with the aid of optimization algorithms", *IET Electric Power Applications*, 12(8), pp. 1067-1074 (2018).

[3] Vukotić, M., Miljavec, D. "Design of a permanent-magnet flux-modulated machine with a high torque density and high power factor", *IET Electric Power Applications*, 10(1), pp. 36-44 (2016).

[4] Asgari, S., Mirsalim, M. "A Novel Dual-Stator Radial-Flux Machine with Diametrically Magnetized Cylindrical Permanent Magnets", *IEEE Trans. Ind. Electron.*, 66(5), pp. 3605 – 3614 (2019).

[5] Feng, C., Jing, X., Bin, G., et al. "Double-stator permanent magnet synchronous in-wheel machine for hybrid electric drive systems", *IEEE Trans. Ind. Electron.*, 45(1), pp. 278–281 (2008).

[6] Mo, L., Quan, L., Zhu, X., et al. "Comparison and analysis of flux-switching permanent-magnet double-rotor machine with 4QT used for HEV", *IEEE Trans. Magn*., 50(11), (2014).

[7] Kim, S., Cho, J., Park, S., et al. "Characteristics comparison of a conventional and modified spoke-type ferrite magnet motor for traction drives of low-speed electric vehicles", *IEEE Trans. Ind. Appl*., 49(6), pp. 2516–2523 (2013).

[8] Dalal A., Kumar, P. "'Design, Prototyping, and Testing of a Dual-Rotor Motor for Electric Vehicle Application", *IEEE Trans. Ind. Electron*, 65(9), pp. 7185-7192 (2018).

[9] Wang, Y., Niu, S., Fu, W. "A Novel Dual-Rotor Bidirectional Flux-Modulation PM Generator for Stand-Alone DC Power Supply", *IEEE Trans. Ind. Electron*, 66(1), pp. 818-828 (2019).

[10] Li, Y., Bobba, D., Sarlioglu, B. "Design and Optimization of a Novel Dual-Rotor Hybrid PM Machine for Traction Application", *IEEE Trans. Ind. Electron*, 65(2), pp. 1762-1771 (2018).

[11] Yang, H., Zhu, Z. Q., Lin, H., et al. "Comparative Study of Hybrid PM Memory Machines Having Single- and Dual-Stator Configurations", *IEEE Trans. Ind. Electron*, 65(11), pp. 9168-9178 (2018).

[12] Baloch, N., Kwon, B., Gao, Y. "Low-Cost High-Torque-Density Dual-Stator Consequent-Pole Permanent Magnet Vernier Machine", *IEEE Trans. Magn*., 54(11), (2018).

[13] Kwon, J. W., Kwon, B. "Investigation of Dual-Stator Spoke-Type Vernier Machine for EV Application", *IEEE Trans. Magn*., 54(11), (2018).

[14] Zhao, W., Chen, D., Lipo, T. A., et al. "Dual Airgap Stator- and Rotor-Permanent Magnet Machines With Spoke-Type Configurations Using Phase-Group Concentrated Coil Windings", *IEEE Trans. Ind. Appl*., 53(4), pp. 3327 – 3335 (2017).

[15] Gao, Y., Qu, R., Li, D., et al. "A Novel Dual-Stator Vernier Permanent Magnet Machine", *IEEE Trans. Magn*, 53(11), (2017).

[16] Gorginpour, H., "Design Modifications for Improving Modulation Flux Capability of Consequent-Pole Vernier-PM Machine in Comparison to Conventional Vernier-PM Machines", Scientia Iranica, (2019).

[17] Baloch, N., Khaliq, S., Kwon, B. I. "HTS dual-stator spoke-type linear Vernier machine for leakage flux reduction", *IEEE Trans. Magn*., 53(11), (2017).

[18] Baloch, N., Khaliq, S., Kwon, B. I. "A high force density HTS tubular Vernier machine", *IEEE Trans. Magn*., 53(11), (2017).

[19] Zhu, L., Jiang, S. Z., Zhu, Z. Q., et al. "Analytical Methods for Minimizing Cogging Torque in Permanent-Magnet Machines", *IEEE Trans. Magn*, 45(4), pp. 2023-2031 (2009).

[20] Hanselman, D. C. "Brushless permanent magnet motor design", McGraw-Hill, New York, (1994).

[21] Gieras, J., Wang, R., Kamper, M. "Axial Flux Permanent Magnet Brushless Machines", Springer-Verlag, New York, (2008).

[22] Zhu, Z. Q., Ruangsinchaiwanich, S., Chen, Y., et al., "Evaluation of superposition technique for calculating cogging torque in permanent-magnet brushless machines", *IEEE Trans. Magn*., 42 (5), (2006).

[23] Sadeghi, S., Parsa, L., "Multiobjective design optimization of five-phase Halbach array permanent-magnet machine" *IEEE Trans. Magn*., 47 (6), (2011).

[24] Gieras, J. F. "Permanent magnet motor technology: design and applications", Taylor & Francis Group, New York, (2010).

[25] Arslan, S. Gurdal, O., Akkaya Oy, S., "Design and Optimization of Tubular Linear Permanent Magnet Generator with Performance Improvement Using Response Surface Methodology and Multi-Objective Genetic Algorithm", Scientia Iranica, (2018).

7. List of Captions

* Figure Captions:

Fig. 1. DMCPMs

Fig. 2. Flux path

Fig. 3. Leakage flux

Fig. 4. One pole pair of the machine MEC

Fig. 5. Simplified MEC,

(**a**) first simplification, **(b)** final

Fig. 6. The PM and stator tooth in a variable thickness PM machine

Fig. 7. The air-gap flux density distribution

Fig. 8. The design process flowchart for DMCPMs

Fig. 9. Magnetic flux density distribution,

(a) initial machine, **(b)** optimized machine

Fig. 10. Back EMF

Fig. 11. Cogging torque

Fig. 12. Electromagnetic torque

* Table Captions:

TABLE 1 The main geometric and electromagnetic parameters of the machine

TABLE 2 The optimization constraints

TABLE 3 The Geometrical parameters

TABLE 4 The initial and optimal design parameters

TABLE 5 The Comparison results

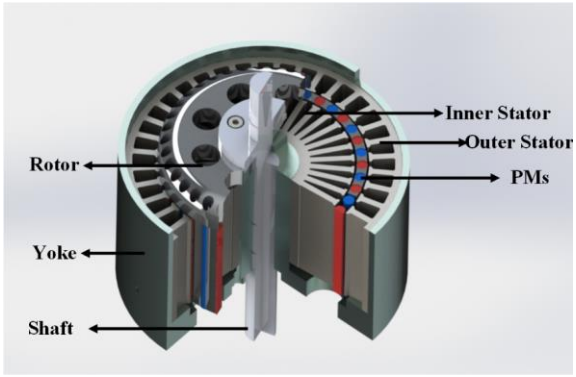

Fig. 1. DMCPMs

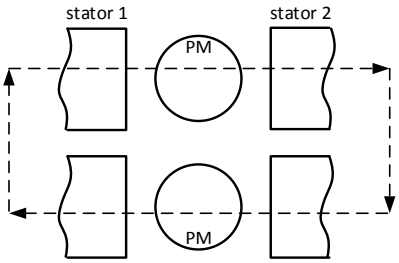

Fig. 2. Flux path

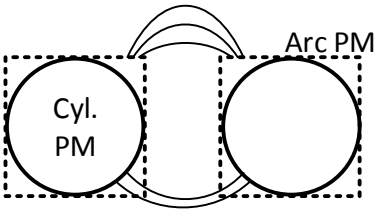

Fig. 3. Leakage flux

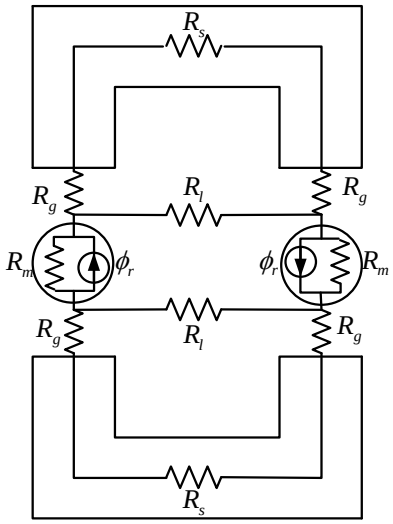

Fig. 4. One pole pair of the machine MEC

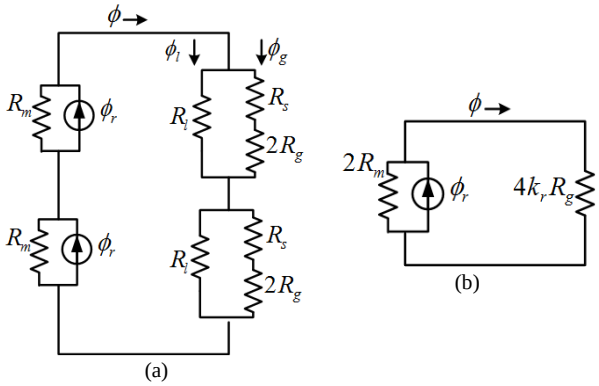

Fig. 5. Simplified MEC,
(a) first simplification, **(b)** final

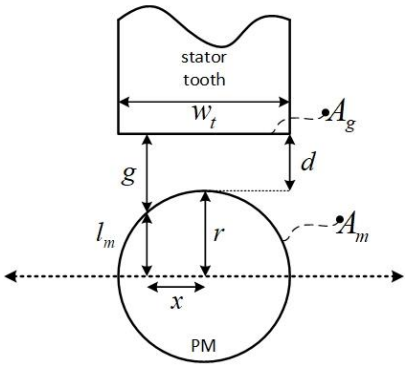

Fig. 6. The PM and stator tooth in a variable thickness PM machine

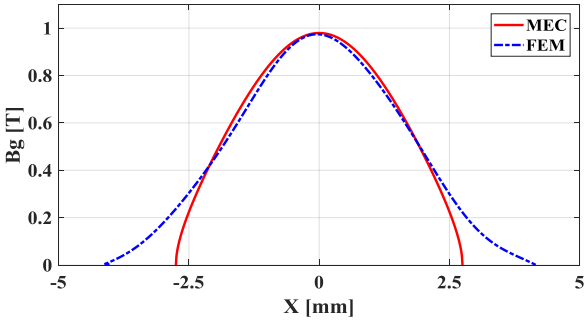

Fig. 7. The air-gap flux density distribution

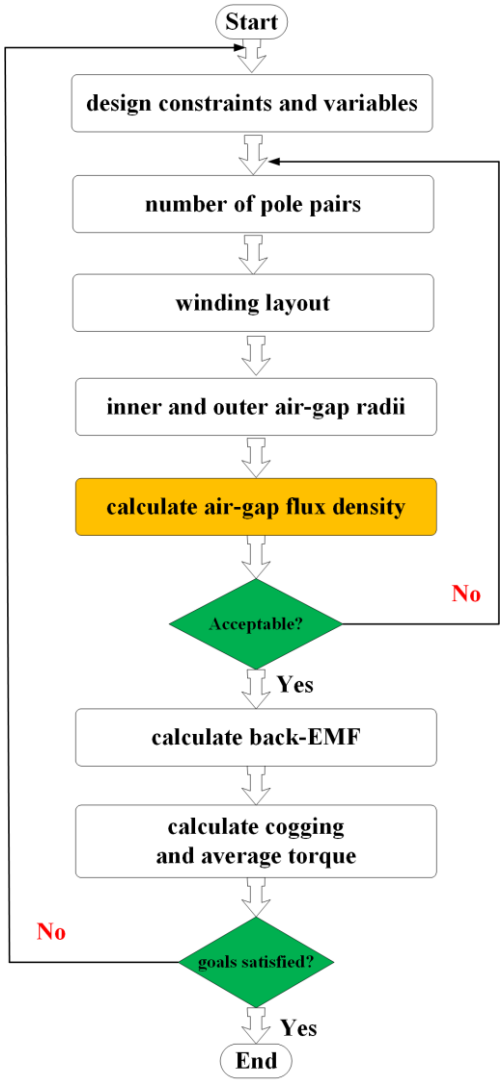

Fig. 8. The design process flowchart for DMCPMs

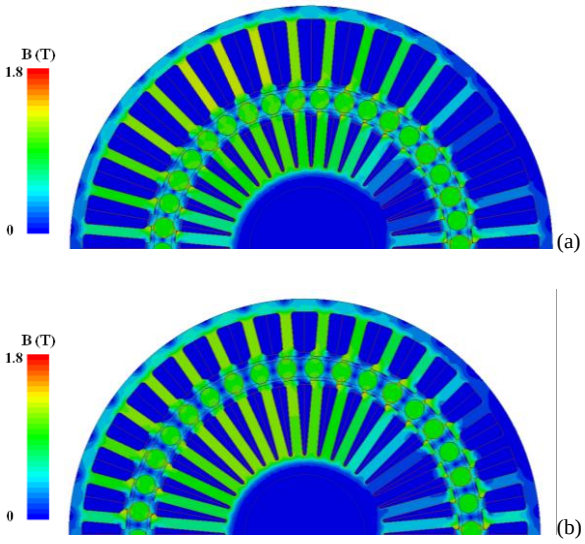

Fig. 9. Magnetic flux density distribution,
(a) initial machine, **(b)** optimized machine

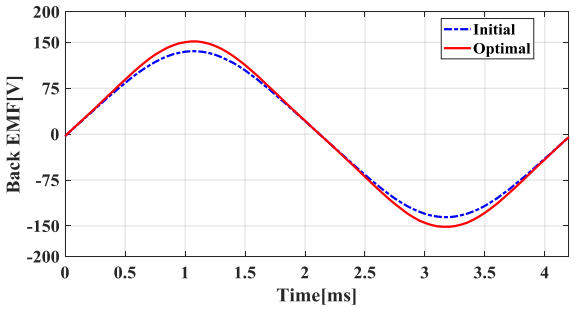

Fig. 10. Back EMF

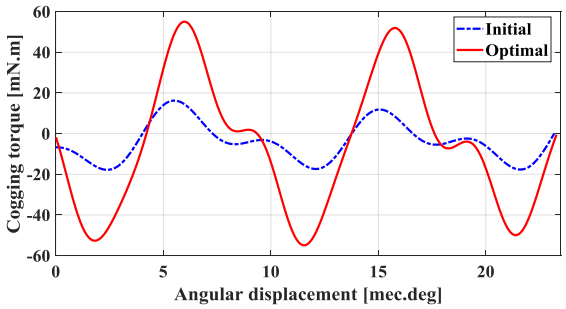

Fig. 11. Cogging torque

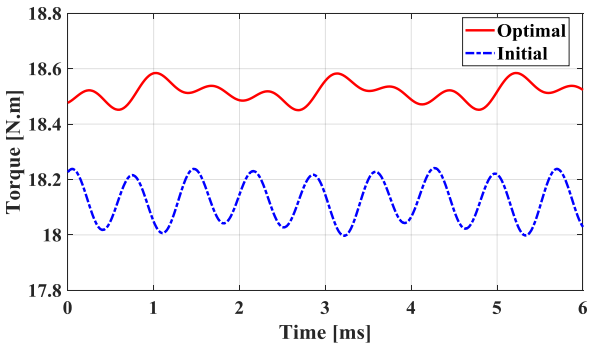

Fig. 12. Electromagnetic torque

TABLE 1 The main geometric and electromagnetic parameters of the machine

Symbol	Parameter	Value
-	Phase	3
-	Slot/pole	36/38
O_D	Motor outer diameter (mm)	133
I_D	Motor inner diameter(mm)	44
d	Minimum air-gap length (mm)	0.7
J	Current density (A/mm^2)	5.5
B_r	PM remanence (T)	1.28
L	Axial length (mm)	60
P_n	Power @750rpm (watt)	1400
r	PM radius (mm)	5.5
K_w	Slot fill factor (%)	50
N	Number of turns of coils	38

TABLE 2 The optimization constraints

Parameter	Value
average torque	> 18.5 Nm
torque ripple	< 1%

TABLE 3 The optimization parameters

Parameter	Initial Value	Optimal Value
rotor diameter(mm)	82	94.1
inner stator tooth width(mm)	3	2.97
outer stator tooth width(mm)	3	3.11

TABLE 4 The initial and optimal design parameters

Parameter	Initial Value	Optimal Value
Torque ripple (%)	1.37	0.8
Cogging torque (%)	0.27	0.7
Torque density (N.m./lit.)	21.75	22.23
Torque density (N.m./kg)	3.895	4.012
Average torque (N.m)	18.12	18.52
Efficiency (%)	91.8	92.4
PM arc to pole arc ratio (α)	0.81	0.7
Machine weight (kg)	4.651	4.616
Core loss (W)	31.2	33
Copper loss (W)	95.9	86.49
Mechanical Power (W)	1427	1445
Back EMF (V)	135.7	151.8
Wire area (mm^2)	0.95	0.86
Phase resistance (ohm)	1.1572	1.2833
Torque per PM volume ($N.m/cm^3$)	0.335	0.343
Slot area (mm^2)	145.44	130.22
Current density (A/mm2)	5.5	5.5

TABLE 5 The Comparison results

Parameter	Machine A	Machine B	Machine C	Machine D
Torque ripple (%)	16	3.2	6.5	0.854
Cogging torque (%)	4	2	-	0.7
Torque density (N.m./lit.)	9.7	6.1	8.7	20.226
Torque density (N.m./kg)	2.4	0.98	-	3.649
Efficiency (%)	90.61	77.2	81	92.69
Current density (A/mm^2)	5	5.2	5.2	5

8. Nomenclature

B_r	magnet remanent flux density	c	air-gap area coefficient
B_g	air-gap flux density	g	air-gap length
ϕ_g	air-gap flux	d	minimum air-gap length
μ_0	permeability of free space	L	axial length
r	PM radius	w_t	tooth width
k_l	leakage factor	k_r	reluctance factor
J	current density	K_w	slot fill factor
A_m	PM cross-section	A_g	air-gap cross-section area
l_m	PM thickness	α	PM arc to pole arc ratio
O_D	motor outer diameter	I_D	motor inner diameter
N_s	number of slots	N_C	smallest common multiplier
C	cogging torque goodness factor	p	number of pole pairs

9. Biography

Shahin Asgari (S'17) was born in Iran, in 1987. He received the B.S. degree from the Kermanshah University of Technology, Iran, in 2012, and the M.S. degree from the Amirkabir University of Technology, Tehran, Iran, in 2015, both in electrical engineering. His research interests include design, analysis, and optimization of electric machines, renewable energy, and hybrid vehicles. He is currently with the Electrical Machines and Transformer Research Laboratory (EMTRL: http://emtrl.aut.ac.ir), Department of Electrical Engineering, Amirkabir University of Technology. Mr. Asgari attained some awards in national/international Robotics competitions, including AUTCUP and Khwarizmi Robotics Competitions.

Reza Yazdanpanah (M'14) received the B.S. degree from Shiraz University, Shiraz, Iran, 2003, the M.S. degree from the Isfahan University of Technology, Isfahan, Iran, 2006, and the Ph.D. degree from Amirkabir University of Technology, Tehran, Iran, 2014, all in electrical power engineering. He is currently an assistant professor in the Department of Electrical Engineering, University of Larestan, Lar, Iran. His research expertise and interests include "Electromagnetic Analysis and Design, Design and simulation of Electrical Machines & Drives, Power Electronics, Power Systems Analysis, Applied Nonlinear Control & Neural Networks". (ryazdanpanah@lar.ac.ir , https://orcid.org/0000-0003-2528-3062)

Mojtaba Mirsalim (SM'04) received the B.S. degree in double major Electrical/Nuclear Engineering and the M.S. degree in nuclear engineering from the University of California, Berkley, in 1978 and 1980, respectively, and the Ph.D. degree in electrical engineering from Oregon State University, Corvallis, in 1986. He is currently a Professor in Electrical Engineering Department. His special fields of interest include design, analysis, and optimization of electric machines.